Vibrational Spectrum of Bathorhodopsin in the Room-Temperature Rhodopsin Photoreaction

F. Jäger, L. Ujj, and G. H. Atkinson*

Contribution from the Department of Chemistry and Optical Science Center, University of Arizona, Tucson, Arizona 85721

Received May 12, 1997. Revised Manuscript Received September 9, 1997[⊗]

Abstract: Picosecond time-resolved coherent anti-Stokes Raman spectroscopy (PTR/CARS) is used to generate high signal to noise (S/N) vibrational spectra of bathorhodopsin (batho) formed in the photoreaction of room-temperature rhodopsin (Rh^{RT}). These PTR/CARS spectra of batho^{RT}, measured as a function of only the time following 3-ps (full width at half maximum), 500-nm excitation of Rh^{RT}, demonstrate that the vibrational structure of batho^{RT} in the 700−1700-cm^{-1} region is distinct from that of Rh^{RT} and remains unchanged over at least the 10 ps [8 ps cross correlation time (CCT)] to 100 ns interval of the Rh^{RT} photoreaction. Given the experimental difficulties associated with the irreversibility of the Rh^{RT} photoreaction, these are the first time-resolved vibrational spectra of batho^{RT} over the full 700−1700-cm^{-1} region to be reported. The PTR/CARS spectra taken after 100 ns contain vibrational features other than those assignable to either Rh^{RT} or batho^{RT} (potentially assignable to the blue-shifted intermediate, BSI). Excellent agreement is found between the major features of the Rh^{RT} and batho^{RT} vibrational spectra measured via PTR/CARS and earlier resonance Raman (RR) spectra taken at low temperatures (LT) selected to thermally stabilize (freeze) batho. Comparisons of the C═C stretching mode region reveal a 12-cm^{-1} shift upon batho^{RT} formation (PTR/CARS data), which agrees well with the 13-cm^{-1} shift found for batho trapped at LT (RR data). These vibrational frequency changes also correlate well with the corresponding 38-nm (LT) and 31-nm (RT) shifts observed in the absorption maxima upon the formation of batho, thereby supporting an inverse relationship between C═C frequencies and absorption maxima proposed for retinal proteins. Comparisons of the C═C stretching frequencies at LT and RT reveal a temperature dependence characterized by *red shifts* of 4 cm^{-1} in Rh and 3 cm^{-1} in batho, the direction of which is opposite to the *blue shifts* observed in the visible absorption maxima of Rh (7 nm) and batho (14 nm). This latter observation suggests a stronger interaction of the protein (likely with the counterion Glu-113) with the *all-trans*-retinal in the batho^{RT} structure than in the corresponding static batho^{LT} structure.

A. Introduction

The room-temperature rhodopsin (Rh^{RT}) protein functions to activate transducin during the enzymatic transduction within the visual process following the absorption of light. The Rh protein, containing seven α-helices spanning the lipid bilayer disc membrane, is found in practically all vertebrate rod and cone cells, as well as in some invertebrates. Light activation in Rh is attributable at the molecular level to the 11-*cis* to *all-trans* isomerization of the retinal chromophore,[1] which occurs in the subpicosecond (200 fs) time range.[2,3] Subsequent structural changes appearing on the ground-state potential surface transfer about 33 kcal/mol[4,5] of energy originally stored in bathorhodopsin (batho) through a sequence of intermediates to finally produce the meta II species, the light-activated form of Rh^{RT}. At the molecular level, the retinal isomerization is eventually converted into structural changes involving the exposure of three cytoplasmic loops (LOOP region)[6] to the transducin coupling mechanism at the surface of the protein.

The 11-*cis*-retinal chromophore is spatially accommodated in the retinal binding pocket of Rh^{RT} and is bonded to the apoprotein (opsin) via a protonated Schiff-base linkage to Lys-296.[7] Subsequent protein changes have been characterized by a variety of static and time-resolved techniques. Intermediates in the Rh^{RT} photoreaction were initially identified and characterized via their respective ultraviolet/visible absorption spectra at RT and at low temperatures (LT) selected to trap specific Rh intermediates.[8−11] A molecular mechanism describing the initial steps in the Rh^{RT} photoreaction has been proposed.[3,12] Specifically, in contrast to bacteriorhodopsin (BR), no photophysical intermediate is formed directly from the Franck−Condon (FC) exited state(s) populated optically (S_1*). Rather, the FC wave packet on S_1* accelerates out of the FC region and crosses coherently within 200 fs into the first photochemical, ground-state intermediate. Subsequent thermal relaxation on the ground state leads to the sequential formation of the batho, blue-shifted intermediate (BSI), lumi, meta I, meta II, and meta III photochemical intermediates. Reactions between some of these intermediates (e.g., batho ⇄ BSI and meta I ⇄ II) have been postulated.[13,14]

* Author to whom correspondence should be addressed.

⊗ Abstract published in *Advance ACS Abstracts,* December 1, 1997.

(1) Wald, G. *Science* **1968**, *162*, 230.
(2) Schoenlein, R. W.; Peteanu, L. A.; Mathies, R. A.; Shank, C. V. *Science* **1991**, *254*, 412−415.
(3) Wang, Q.; Schoenlein, R. W.; Peteanu, L. A.; Mathies, R. A.; Shank, C. V. *Science (Washington, DC)* **1994**, *266*, 422−424.
(4) Schick, G. A.; Cooper, T. M.; Holloway, R. A.; Murray, L. P.; Birge, R. R. *Biochemistry* **1987**, *26*, 2556.
(5) Cooper, A. *Nature* **1979**, *282*, 531−533.
(6) Koenig, B.; Arendt, A.; McDowell, J. H.; Kahlert, M.; Hargrave, P. A.; Hofmann, K. P. *Proc. Natl. Acad. Sci. U.S.A.* **1989**, *86*, 6878−6882.
(7) Ovchinnikov, Y. A. *FEBS Lett.* **1982**, *148*, 179−191.
(8) Kliger, D. S.; Lewis, J. W. *Isr. J. Chem.* **1995**, *35*, 289−307.
(9) Lewis, J. W.; Kliger, D. S. *J. Bioenerg. Biomembr.* **1992**, *24*, 201−210.
(10) Kandori, H.; Shichida, Y.; Yoshizawa, T. *Biophys. J.* **1989**, *56*, 453−457.
(11) Peteanu, L. A.; Schönlein, R. W.; Wang, Q.; Mathies, R. A.; Shank, C. V. *Proc. Natl. Acad. Sci. U.S.A.* **1993**, *90*, 11762−11766.
(12) Kochendoerfer, G. G.; Mathies, R. A. *Isr. J. Chem.* **1995**, *35*, 211−226.

S0002-7863(97)01529-1 CCC: $14.00

Molecular changes have been monitored by static[15,16] and time-resolved[17,18] resonance Raman (RR) and Fourier transform infrared (FTIR)[19,20] techniques, by electron microscopic techniques,[21] and by NMR techniques.[22,23] Most of the reported work has focused either on the late intermediates (i.e., meta I and meta II) and their influence on the activation mechanism or on LT measurements of the early photoreaction intermediates (i.e., batho, lumi, and meta I) that can be thermally trapped. FTIR data provide evidence that Glu-113 is the counterion in the Rh^{RT} photoreaction,[24,25] while NMR results have located the counterion within the protein adjoining the retinal.[23] RR studies characterized and assigned normal modes in retinal,[26] Rh^{RT},[27] and $batho^{LT}$.[28,29] Transient ultraviolet and visible absorption spectroscopy on Rh^{RT} samples containing both native and modified retinals have identified the intermediates comprising the Rh^{RT} photoreactions.[8,10,30,31] Time-resolved fluorescence studies have determined the excited-state lifetime of Rh^{RT} [32,33] and of the 11-*cis* chromophore in solution.[34]

Since it is experimentally difficult to measure high signal to noise (S/N) data from intermediates in an irreversible photoreaction such as that in Rh^{RT} (unlike BR), Atkinson and coworkers have developed coherent anti-Stokes Raman spectroscopy (CARS) in a time-resolved instrumental configuration appropriate for applications to protein reactions.[35−39] The picosecond time-resolved CARS (PTR/CARS) techniques and methodologies were developed initially to examine the intermediates comprising the reversible BR^{RT} photocycle and subsequently, have been applied to intermediates in the irreversible Rh^{RT} photoreaction.[17,18] These PTR/CARS spectra have been recorded from BR^{RT} and Rh^{RT} over time intervals ranging from <5 ps to several hundred nanoseconds.[40,41] The first PTR/CARS vibrational data from batho were restricted to spectral regions containing the hydrogen-out-of-plane (HOOP) and ethylenic (C═C) stretching modes.[18] Several recent experimental and instrumental improvements have led to PTR/CARS data with significantly better S/N that are measurable over the spectral range from 700 to 1700 cm^{-1}.

In this paper, emphasis is given to obtaining reliable, high S/N data on the vibrational degrees of freedom of batho at physiological temperatures during the Rh^{RT} photoreaction and to compare these results with RR data measurement from $batho^{LT}$. These PTR/CARS results demonstrate that the structure of batho does not change from 10 ps to 100 ns, at which time $batho^{RT}$ decays into an equilibrium with BSI.[8] In spectra taken more than 100 ns after the 3-ps, 500-nm laser excitation of Rh^{RT}, some contributions from species other than Rh^{RT} and $batho^{RT}$ are observed, a result that will be investigated in more detail elsewhere.[42]

B. Materials and Methods

Bovine retina (Lawson Company, Lincoln, NE) are prepared in accordance with published procedures.[43] Washed Rh membranes are resuspended in 10 mM Tris buffer (pH 7) with aprotinin (0.1% v/v) and dithiothreitol (DTT). Purified Rh samples are characterized by a ratio of the absorption intensities at 280 nm versus 500 nm of about 2. The optical density (OD) of the Rh sample at 500 nm (with background scattering subtracted) is adjusted to be ≈3 OD. The remaining Rayleigh scattering from the disc membranes is measured to have an ≈2 OD at 800 nm. The sample volume is typically 25−30 mL to ensure a constant Rh concentration while a spectrum is recorded (20−30 s). To improve the S/N, two consecutively measured PTR/CARS spectra are added. This procedure maintains a constant Rh concentration (within $<5\%$) and thereby ensures the fidelity of the respective amplitudes and line shapes.

Since a detailed description of the experimental setup and the formulas used for the nonlinear $\chi^{(3)}$ analysis is described elsewhere,[39,41] only a brief summary is presented here. A mode-locked, Nd−YLF laser (Coherent, Antares 76 YLF) generates 30-ps pulses at 1054 nm that are used to generate second and third harmonic (Coherent 7950 THG) outputs from KTP (527 nm) and BBO (351 nm) crystals, respectively. The 527-nm and 351-nm beams are used to pump three, independently controlled dye lasers (Coherent, Model 700). Each dye laser is equipped with a cavity dumper (Coherent, Models 7210 and 7220), all three of which are synchronized to the 76-MHz rate of the Nd−YLF mode locker. Typically, the laser system is operated at a 400-kHz repetition rate that is selected to match the experimental conditions used to create the liquid sample jet. Specifically, the velocity in the 400 μm square nozzle is adjusted to >12 m/s to ensure a complete replacement of the sample volume between the arrival of sequential sets of three picosecond laser pulses (determined by the 20-μm beam waist of the pump beam and the 400 kHz repetition rate).

Procedurally, two parallel sample nozzles are used in order to permit the nonresonant background signal (water or buffer) to be measured simultaneously with the PTR/CARS signal from Rh. This is accomplished by directing the CARS beams generated in the reference

(13) Thorgeirsson, T. E.; Lewis, J. W.; Wallace-Williams, S. E.; Kliger, D. S. *Biochemistry* **1993**, *32*, 13861−13872.
(14) Lewis, J. W.; Pinkas, I.; Sheves, M.; Ottolenghi, M.; Kliger, D. S. *J. Am. Chem. Soc.* **1995**, *117*, 918−923.
(15) Mathies, R. A.; Smith, S. O.; Palings, I. Determination of retinal chromophore structure in rhodopsins. In *Biological Applications of Raman Spectroscopy*; Spiro, T. G., Ed.; John Wiley & Sons: New York, 1987; Chapt. 2, pp 59−108.
(16) Callender, R. H.; Honig, B. *Annu. Rev. Biophys. Bioeng.* **1977**, *6*, 33−55.
(17) Popp, A.; Ujj, L.; Atkinson, G. H. *Biophys. Chem.* **1995**, *56*, 129−135.
(18) Popp, A.; Ujj, L.; Atkinson, G. H. *Proc. Natl. Acad. Sci. U.S.A.* **1996**, *93*, 372−376.
(19) Siebert, F. *Isr. J. Chem.* **1995**, *35*, 309−323.
(20) Degrip, W. J.; Gray, D.; Gillespie, J.; Bovee, P. H. M.; van den Berg, E. M. M.; Lugtenburg, J.; Rothschild, K. J. *Photochem. Photobiol.* **1988**, *48*, 497−504.
(21) Schertler, G. F. X.; Villa, C.; Henderson, R. *Nature (London)* **1993**, *362*, 770−772.
(22) Han, M.; DeDecker, B. S.; Smith, S. O. *Biophys. J.* **1993**, *65*, 899−906.
(23) Han, M.; Smith, S. O. *Biochemistry* **1995**, *34*, 1425−1432.
(24) Fahmy, K.; Jäger, F.; Beck, M.; Zvyaga, T. A.; Sakmar, T. P.; Siebert, F. *Proc. Natl. Acad. Sci. U.S.A.* **1993**, *90*, 10206−10210.
(25) Jäger, F.; Fahmy, K.; Sakmar, T. P.; Siebert, F. *Biochemistry* **1994**, *33*, 10878−10882.
(26) Curry, B.; Broek, A.; Lugtenburg, J.; Mathies, R. A. *J. Am. Chem. Soc.* **1982**, *104*, 5274−5286.
(27) Eyring, G.; Curry, B.; Broek, A.; Lugtenburg, J.; Mathies, R. *Biochemistry* **1982**, *21*, 384−393.
(28) Palings, I.; van den Berg, E. M. M.; Lugtenburg, J.; Mathies, R. A. *Biochemistry* **1989**, *28*, 1498−1507.
(29) Palings, I.; Pardoen, J. A.; van den Berg, E. M. M.; Winkel, C.; Lugtenburg, J.; Mathies, R. A. *Biochemistry* **1987**, *26*, 2544−2556.
(30) Mizukami, T.; Kandori, H.; Shichida, Y.; Chen, A.-H.; Derguini, F.; Caldwell, C. G.; Bigge, C. F.; Nakanishi, K.; Yoshizawa, T. *Proc. Natl. Acad. Sci. U.S.A.* **1993**, *90*, 4072−4076.
(31) Nakanishi, K.; Chen, A.-H.; Derguini, F.; Franklin, P.; Hu, S.; Wang, J. *Pure Appl. Chem.* **1994**, *66*, 981−988.
(32) Kochendoerfer, G. G.; Mathies, R. A. *J. Phys. Chem.* **1996**, *100*, 14526−14532.
(33) Doukas, A. G.; Junnarkar, M. R.; Alfano, R. R.; Callender, R. H. *Biophys. J.* **1985**, *47*, 795−798.
(34) Kandori, H.; Katsuta, Y.; Ito, M.; Sasabe, H. *J. Am. Chem. Soc.* **1995**, *117*, 2669−2670.
(35) Ujj, L.; Atkinson, G. H. *Isr. J. Chem.* **1993**, *33*, 207−214.
(36) Ujj, L.; Jäger, F.; Popp, A.; Atkinson, G. H. *Chem. Phys.* **1996**, *212*, 421−436.
(37) Jäger, F.; Ujj, L.; Atkinson, G. H.; Sheves, M.; Livnah, N.; Ottolenghi, M. *J. Phys. Chem.* **1996**, *100*, 12066−12075.
(38) Ujj, L.; Popp, A.; Atkinson, G. H. *Chem. Phys.* **1994**, *188*,221−234.
(39) Ujj, L.; Volodin, B. L.; Popp, A.; Delaney, J. K.; Atkinson, G. H. *Chem. Phys.* **1994**, *182*, 291−311.
(40) Weidlich, O.; Ujj, L.; Jäger, F.; Atkinson, G. H. *Biophys. J.* **1997**, *72*, 2329−2341.
(41) Ujj, L.; Jäger, F.; Atkinson, G. H. *Biophys. J.* **1997**. In press.
(42) Ujj, L.; Jäger, F.; Atkinson, G. H., manuscript in preparation.
(43) Papermaster, D. S. *Methods Enzymol.* **1982**, *81*, 49−52.

and sample jets into the filter stage of a triple monochromator (Spex triplemate) in order to project two separated parallel signals onto the liquid nitrogen-cooled CCD array (Princeton Instruments LN/CCD-1024-F/1UV).

Initially, picosecond (pulsed) resonance CARS (PR/CARS) spectra are recorded from Rh^{RT} under conditions that ensure a constant concentration. PTR/CARS spectra are obtained at selected time delays following the 500-nm (3-ps, 7 nJ/pulse) excitation (ω_p) of Rh^{RT}. The order in which PR/CARS and PTR/CARS spectra are recorded is alternated in order to minimize the effect of the concentration decrease in the Rh^{RT} sample due to the irreversibility of the photoreaction. Two probe laser pulses (8-ps CCT), ω_1 and ω_s, are tuned to either 600 and 640 nm (HOOP and fingerprint) or 600 and 653 nm (fingerprint and C═C) to generate CARS signals in these respective regions from the Rh^{RT}/batho^{RT} photoreaction mixture. The Stokes laser, ω_s, determines that the spectral range measured with a set of ω_1 and ω_s pulses has a 700-cm^{-1} width. The spectral resolution of the entire detection system (triple monochromator and multichannel analyzer) is controlled by several spectroscopic parameters, including the spacing between pixels on the CCD, and is measured to be <0.5 cm^{-1} (i.e., wavenumber separation between two data points). The overall spectral resolution, determined by the convolution of the resolution from the detection system and the line shape of the ω_1 laser, is estimated to be <2 cm^{-1}. The error in measuring the wavenumber position of a given vibrational feature is <1 cm^{-1} for Rh^{RT} and <2 cm^{-1} for batho^{RT} throughout the 700−1600-cm^{-1} region. For vibrational features above 1600 cm^{-1}, the intensity of the Stokes laser decreases, as does the associated S/N, thereby leading to a slightly larger error, *vide infra*.

Three independently operated optical delay lines are used to determine the timing sequence with which the three dye laser pulses arrive at the sample jet. Time delays between the pump (ω_p) and probe (ω_1 and ω_s) pulses are selected by optical delays to range from several picoseconds to 1 ns. For time delays between 13 and 104 ns, the cavity dumper controllers are used to electronically delay both ω_1 and ω_s from ω_p in multiple periods of 13 ns. In order to efficiently generate coherent scattering, the angles by which the ω_1, ω_p, and ω_s laser beams transverse the sample jet are selected by the beam steering optics to fulfill the phase-matching, **k**-vector geometry.

The optical excitation of Rh^{RT} is estimated to result in a 35−40% conversation into intermediates. This value is determined from the amplitude decrease in vibrational features assigned to Rh^{RT}, i.e., the decrease of the corresponding $\chi^{(3)}$ fit parameter for Rh^{RT}. For analyzing the PTR/CARS data, the spectrum from Rh^{RT} in buffer is normalized to the nonresonant background originating from the water (buffer) alone. The instrumental response, including the spectral characteristics of the broadband (ω_s) laser, is considered in the data analysis, as is the amplitude stability of the ω_1 and ω_s lasers themselves. Both of the latter points can be controlled by recording (i) a spectrum from the flowing jet sample of the Rh^{RT} and the reference (buffer only) at the beginning of each experiment and (ii) spectra from the Rh^{RT} sample and reference simultaneously throughout each set of PR/CARS and PTR/CARS measurements. This procedure ensures that one set of unique $\chi^{(3)}$ parameters can be used to quantitatively fit both the PR/CARS and PTR/CARS data taken within the same series of measurements.

C. Results

The PR/CARS data from Rh^{RT} and the PTR/CARS results assignable to batho^{RT} are shown together with their respective $\chi^{(3)}$ fitting functions for the 700−1700 cm^{-1} region in Figures 1−6. The $\chi^{(3)}$ fitting parameters (i.e., band positions Ω_i, bandwidths Γ_i, and amplitudes A_i) for Rh^{RT} and batho^{RT} are also presented in Tables 1 and 2, respectively. In general, the $\chi^{(3)}$ model function is selected to find the minimum number of bands needed to fit the CARS data while maintaining an error of $<3\%$.

PR/CARS Data for Rh^{RT}. In general, the PR/CARS bands assigned to Rh^{RT} (Figures 1 and 3) are in excellent agreement with RR results published earlier[27−29,44] (i.e., at most, 3-cm^{-1} differences). These differences may be due in part to variations in the origin positions determined in CARS analysis relative to the band maxima positions derived in RR data. Although the

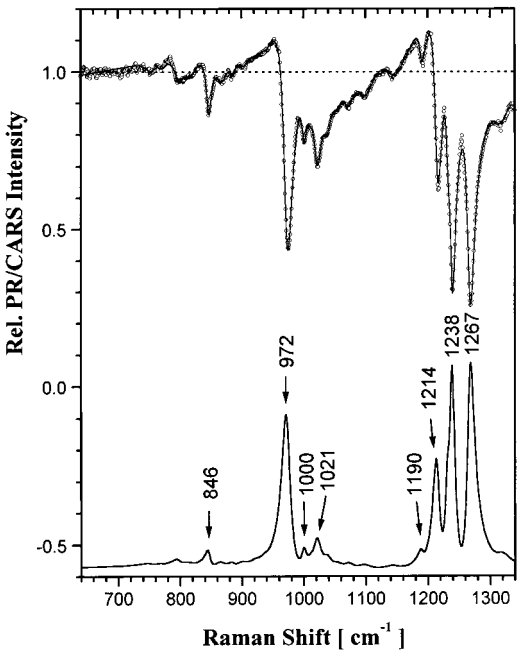

Figure 1. PR/CARS spectrum of Rh^{RT} (3.5 OD sample) in the 640−1400-cm^{-1} range. The nonresonant CARS background signal from water and opsin is used to normalize the PR/CARS signal to 1. The $\chi^{(3)}$-fit function, modeling both the resonance term and the nonresonant background, is shown as a solid line over the PR/CARS data (○). The corresponding vibrational spectrum of Rh^{RT} derived from the $\chi^{(3)}$ fit using a Lorentzian band-shape function is shown at the bottom. The wavenumber positions of selected bands are also presented.

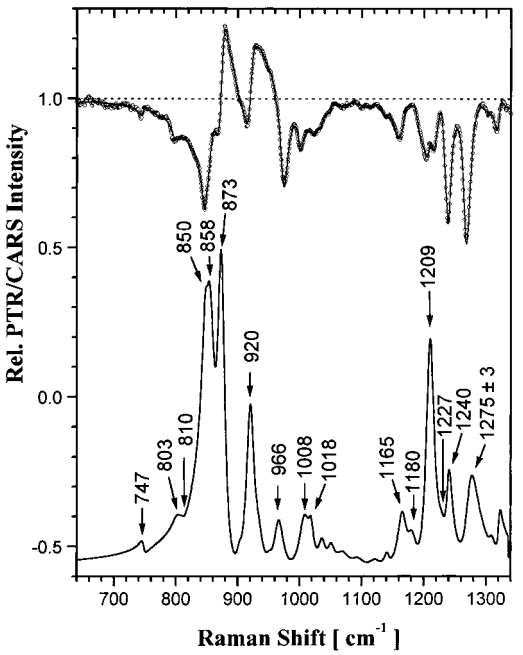

Figure 2. PTR/CARS spectrum in the 640−1340-cm^{-1} range of the reaction mixture containing Rh^{RT} and the intermediate batho^{RT} (ca 35−40% relative concentration) taken 20 ps after photoexcitation. The nonresonant background signal from water and opsin is used to normalize the PR/CARS signal to 1. The $\chi^{(3)}$ fit function, modeling the resonance terms of Rh and batho and the background, is shown as a solid line over the PTR/CARS data (○). The corresponding vibrational spectrum of batho^{RT}, derived from the $\chi^{(3)}$ fit using a Lorentzian band-shape function, is shown at the bottom. The wavenumber positions of selected bands are also presented.

(44) Deng, H.; Callender, R. H. *Biochemistry* **1987**, *26*, 7418−7426.

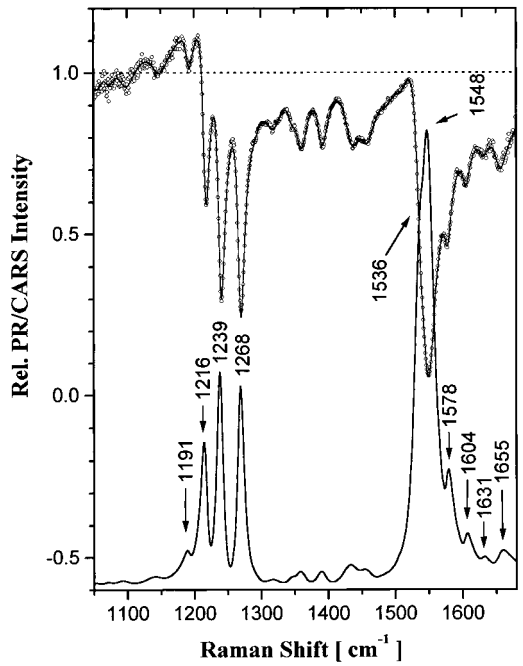

Figure 3. PR/CARS spectrum of Rh^{RT} (3.5 OD sample) in the 960−1700-cm^{-1} range. The nonresonant CARS background signal from water and opsin is used to normalize the PR/CARS signal to 1. The $\chi^{(3)}$-fit function, modeling both the resonance term and the nonresonant background, is shown as a solid line over the PR/CARS data (○). The corresponding vibrational spectrum of Rh^{RT}, derived from the $\chi^{(3)}$ fit using a Lorentzian band-shape function, is shown at the bottom. The wavenumber positions of selected bands are also presented.

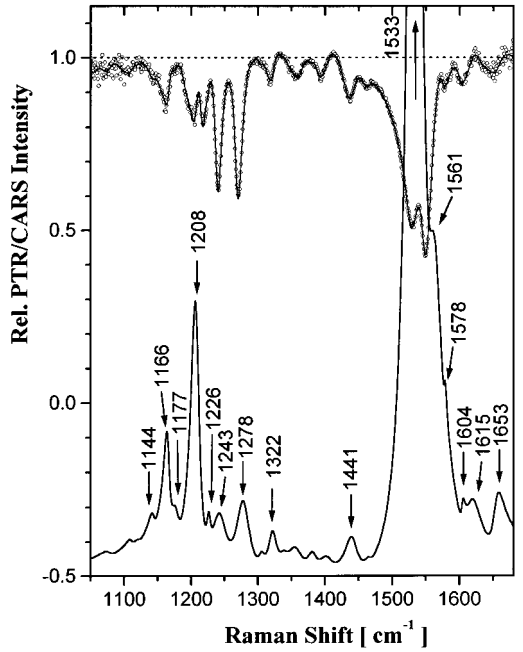

Figure 4. PTR/CARS spectrum in the 960−1680-cm^{-1} range of the reaction mixture containing Rh^{RT} and the intermediate $batho^{RT}$ (ca 35−40% relative concentration) taken 20 ps after photoexcitation. The nonresonant background signal from water and opsin is used to normalize the PR/CARS signal to 1. The $\chi^{(3)}$ fit function, modeling the resonance terms of Rh and batho and the background, is shown as a solid line over of the PTR/CARS data (○). The corresponding vibrational spectrum of Rh^{RT}, derived from the $\chi^{(3)}$ fit using a Lorentzian band-shape function, is shown at the bottom. The wavenumber positions of selected bands are also presented.

ethylenic (C═C) stretching modes in Rh^{RT} have been assigned to a single band at 1546 cm^{-1} [29,45] or at 1545 cm^{-1},[46] the $\chi^{(3)}$

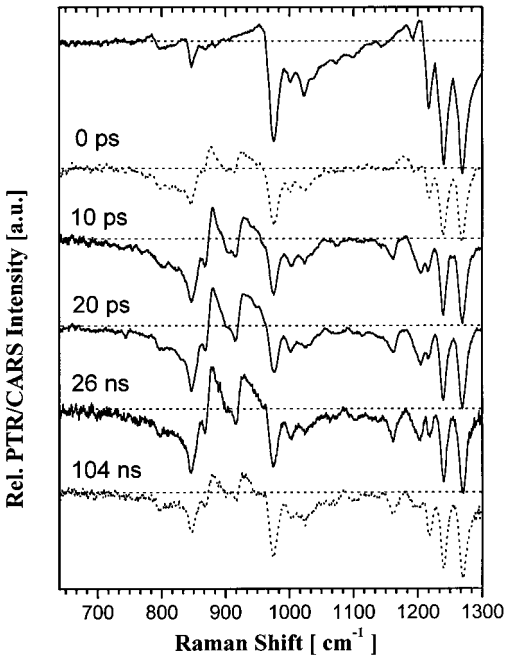

Figure 5. PR/CARS spectrum of Rh^{RT} and PTR/CARS spectra of the Rh^{RT}/$batho^{RT}$ mixture, both in the 640−1300-cm^{-1} region, are measured at 0 ps (8 ps CCT), 10 ps, 20 ps, 26 ns, and 104 ns following 3 ps, 500-nm (7.5 nJ) photoexcitation. The dotted line spectra at 0 ps and 104 ns contain minimal contributions from $batho^{RT}$, while those recorded at 10 ps, 20 ps, and 26 ns contain significant contributions from $batho^{RT}$. The horizontal, dashed lines in each spectrum represent the resonant background CARS signal.

-analysis reveals that the CARS feature at 1545 cm^{-1} is best fit by two bands (at 1536 and 1548 cm^{-1}, with the latter having the larger amplitude). For comparisons of C═C stretching features, this band is referenced as appearing at 1545 cm^{-1}; *vide infra*.

Only in the RR spectrum of *all-trans*-retinal have individual C═C modes been assigned firmly: 1577 cm^{-1} (C_{11}═C_{12}), 1569 cm^{-1} (C_9═C_{10}), and 1550 cm^{-1} (C_{13}═C_{14}) and tentatively at 1611 cm^{-1} (C_5═C_6) and 1594 cm^{-1} (C_7═C_8).[26] In vibrational spectra from pigments (e.g., Rh), the strong overlap between these bands, together with the differences in Raman cross sections, characteristically results in the appearance of one central band (containing the major intensity) flanked by at least two separate bands of lower intensities. In the RR spectrum of Rh^{LT}, C═C stretching modes have been assigned to bands at 1549, 1582, 1599, 1609, and 1636 cm^{-1}.[44] Most of these RR bands are of a symmetric [(C═C)$_+$] rather than of antisymmetric [(C═C)$_-$] character. The (C═C)$_-$ features become prominent only if the retinal interacts strongly with the protein environment.[47]

The Schiff-base C═N stretching mode appears at 1655 cm^{-1} in PR/CARS data, at 1657 cm^{-1} in RR spectra at LT,[44] and at 1656 cm^{-1} in RR spectra at RT[29] (647-nm probe).

PTR/CARS Data for $Batho^{RT}$. The results obtained from the PTR/CARS data assignable to $batho^{RT}$ (Figures 4 and 5) are described in detail for three separate vibrational regions.

(a) Hydrogen-out-of-Plane (HOOP) Region. The vibrational features assignable to the HOOP modes, appearing in the 700−1000-cm^{-1} region, are essentially the same as those in

(45) Mathies, R. A.; Oseroff, A. R.; Stryer, L. *Proc. Natl. Acad. Sci. U.S.A.* **1976**, *73*, 1−5.
(46) Callender, R. H.; Doukas, A. G.; Crouch, R. K.; Nakanishi, K. *Biochemistry* **1976**, *15*, 1621−1629.
(47) Birge, R. R.; Einterz, C. M.; Knapp, H. M.; Murray, L. P. *Biophys. J.* **1988**, *53*, 367−385.

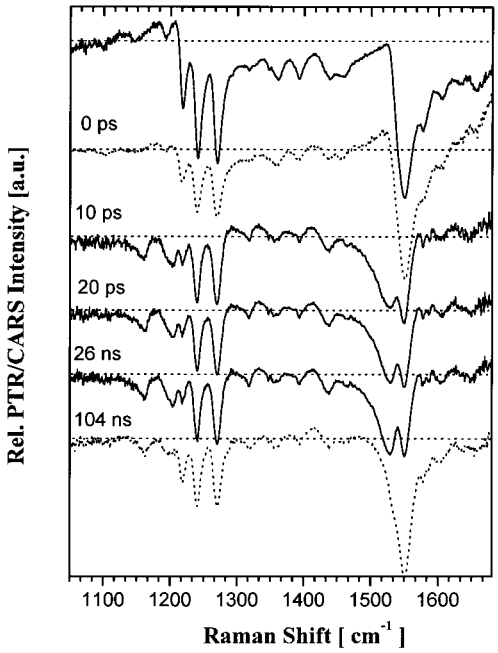

Figure 6. PR/CARS spectrum of Rh^{RT} and PTR/CARS spectra of the Rh^{RT}/batho^{RT} mixture, both in the 1050−1680-cm^{-1} region of the Rh^{RT}/batho^{RT} mixture are measured at 0 ps (8 ps CCT), 10 ps, 20 ps, 26 ns, and 104 ns following 3 ps, 500-nm (7.5 nJ) photoexcitation. The dotted line spectra at 0 ps and 104 ns contain minimal contributions from batho^{RT}, while those recorded at 10 ps, 20 ps, and 26 ns contain significant contributions from batho^{RT}. The horizontal, dashed lines in each spectrum represent the resonant background CARS signal

the RR and PTR/CARS spectra reported to date. It is valuable to note that two bands, at 850 and 858 cm^{-1}, are definitely resolved in the PTR/CARS data presented here (given the <5% error limit).

(b) Fingerprint Region. The C−C stretching regions observed in RR and PTR/CARS data differ in two ways. The band at 1278 cm^{-1} is not accompanied by a 1265-cm^{-1} band.[29,44] In addition, unlike the RR spectrum, there is no band found in PTR/CARS spectra at 1214 cm^{-1} (assigned to the C_8−C_9 stretch in LT/RR data).[29]

The intensity of the 1240-cm^{-1} band (C_{12}−C_{13} stretch) varies relative to the RR data previously reported.[29,44] Only one of these results[44] agrees well with that from PTR/CARS spectra. This difference may be attributable to subtraction errors involving the LT mixture containing Rh, isorhodopsin, and batho, especially since the 1240-cm^{-1} band is present in the vibrational spectra of all three species.

(c) Ethylenic Region. Compared to RR data at LT,[29,44] where it appears at 1536 cm^{-1}, the most intense C═C stretching feature is shifted 3 cm^{-1} to lower energy in PTR/CARS spectra and appears at 1533 cm^{-1}. The position of the C═N stretching mode in PTR/CARS, 1653 cm^{-1}, compares well with the corresponding RR bands recorded at LT that appear at 1657 cm^{-1} [44] and 1654 cm^{-1}.[29]

Differences in the positions of weak features located between the C═C and C═N stretching bands are observed. In PTR/CARS data from batho^{RT}, a shoulder on the high-energy side of the C═C band is found at 1561 cm^{-1}, whereas bands at 1577, 1595, and 1629 cm^{-1} have been assigned in earlier work.[44] The positions and relative amplitudes of these bands vary somewhat between Palings et al.[29] and Deng and Callender.[44] Since data from this region contain more spectral noise than that found in other regions, only the 1561-cm^{-1} band is recognized as a significant feature. Three additional bands appear at 1578, 1604, and 1615 cm^{-1}, but the position of each is considered to be uncertain (±5 cm^{-1}) given the noise.

Table 1. Parameters Describing the $\chi^{(3)}$ Fits to the PR/CARS and PTR/CARS Data in the Wavenumber Range from 640 to 1340 cm^{-1} for Rhodopsin and Bathorhodopsin[a]

rhodopsin PR/CARS			bathorhodopsin PTR/CARS		
Ω_i (cm^{-1})	Γ_i (cm^{-1})	A_i	Ω_i (cm^{-1})	Γ_i (cm^{-1})	A_i
752	9	0.015	747	5	0.02
770	7	0.010			
780	7	0.029	803	6	0.01
814	15	0.034	810	6	0.01
846	5	0.097	850	7	0.073
867	11	0.053	858	9	0.12
883 ± 2	6	0.030	873	7	0.19
900 ± 3	10	0.030	904	5	0.012
923	10	0.019	920	7	0.14
938	8	0.025	930	9	0.037
972	9	0.42	966	9	0.058
1000	5	0.083			
1010	7	0.054	1008	8	0.064
1021	8	0.16	1018	6	0.043
1035 ± 2	8	0.065	1035	7	0.037
1050 ± 3	11	0.046	1050	7	0.032
1071	9	0.055	1068	7	0.023
1097	15	0.050	1088	10	0.016
			1120 ± 3	12	0.009
1145 ± 3	15	0.055	1140	6	0.012
			1165	6	0.064
1190	9	0.088	1180	11	0.050
1214	7	0.33	1209	8	0.18
1232	4	0.15	1227	4	0.04
1238	5	0.41	1240	4	0.076
1267	7	0.46	1275 ± 3	10 ± 4	0.091
1316	12	0.058	1321	5	0.041

[a] Ω_i band origin, Γ_i bandwidth HWHM, and A_i amplitudes are shown. The values for the PR/CARS amplitudes represent typical values for a 3−4 OD sample if the spectrum is normalized to the nonresonant CARS background. The values for the PTR/CARS amplitudes correspond to a 3−4 OD sample with 35−40% conversion to intermediates via optical excitation. The electronic phase factor is $\Theta = (65 \pm 5)°$ for Rh^{RT} and $\Theta = (170 \pm 10)°$ for batho^{RT}. The $(A_i)^2$ values correspond to the relative intensities shown in the background-free spectra for isolated features.

Comparison of PTR/CARS Results. The first PTR/CARS spectra from batho^{RT} have been recorded over a limited spectral region and exhibited a lower S/N than obtained in the present study.[18] The small C═C spectral range available in the earlier measurements (250 cm^{-1}) restricted the opportunity to find a unique parameter set for the $\chi^{(3)}$ relationship used to fit the PTR/CARS data. Two reasons for this restriction can be identified:

(a) The $\chi^{(3)}$ fitting function must simultaneously fit the dispersively shaped PTR/CARS bands to a complex Lorentzian function, which is multiplied by a second-order polynomial in order to account for the normalized nonresonant background. This opportunity is enhanced in the PTR/CARS data presented here since the spectral region measured is much larger (about 700 cm^{-1}). In addition, both spectral regions from which data are recorded in this work encompass the entire 700−1700-cm^{-1} region and overlap strongly, thereby permitting accurate normalization of band intensities.

(b) The unavailability of a third, independently controlled dye laser in the earlier experiments restricted the choice of the second probe laser wavelength, thereby experimentally limiting the phase value. Secondarily, the types of dispersive line shapes found in the PTR/CARS data are also restricted.

Collectively, the effects of the factors described above make it more difficult to separate the PTR/CARS spectra into Rh^{RT} and batho^{RT} components. The impact of the new results on the energy storage/transduction mechanism is discussed in more detail below.

Table 2. Parameters Describing the $\chi^{(3)}$ Fits to the PR/CARS and PTR/CARS Data in the Wavenumber Range from 1050 to 1680 cm^{-1} for Rhodopsin and Bathorhodopsin[a]

rhodopsin PR/CARS			bathorhodopsin PTR/CARS		
Ω_i (cm^{-1})	Γ_i (cm^{-1})	A_i	Ω_i (cm^{-1})	Γ_i (cm^{-1})	A_i
1037	6	0.071			
1054	8	0.03			
1072	10	0.03			
1098	15	0.043			
			1121	7	0.008
1148 ± 2	15	0.044	1144	5	0.02
			1166	5	0.084
1191	8	0.057	1177	9	0.049
1216	6	0.28	1208	8	0.20
1239	6	0.42	1226	4	0.032
1268	7	0.41	1243	15	0.081
1290	7	0.029	1278	13	0.099
			1306	5	0.02
1317	16	0.075	1322	8	0.062
1345	8	0.039	1339	8	0.02
1359	10	0.10	1355	14	0.050
1390	11	0.096	1381	8	0.033
			1403	12	0.033
1434	15	0.11	1441	12	0.063
1457	15	0.074	1465	5	0.01
1486	18	0.037			
1507	15	0.033			
1536	11	0.44	1533	12	0.51
1548	10	0.68	1561	12	0.11
1578	7	0.10	~1578	~2	~0.017
1604	7	0.069	~1604	~3	~0.021
1631 ± 2	8	0.030	~1615	~12	~0.042
1655	8	0.065	1653	10	0.063

[a] Ω_i band origin, Γ_i bandwidth HWHM, and A_i amplitudes are shown. The values for the PR/CARS amplitudes represent typical values for a 3−4 OD sample if the spectrum is normalized to the nonresonant CARS background. The values for the PTR/CARS correspond to a 3−4 OD sample with 35−40% conversion to intermediates via optical excitation. The electronic phase factor is $\Theta = (69 \pm 5)°$ for Rh^{RT} and $\Theta = (168 \pm 10)°$ for $batho^{RT}$. The $(A_i)^2$ values correspond to the relative intensities shown in the background-free spectra for isolated features.

D. Discussion

The vibrational data presented here are the first to be reported for $batho^{RT}$ over the entire 700−1700-cm^{-1} range. A few bands in the HOOP region have been measured previously by single laser excitation and analyzed by subtraction of steady-state Raman spectra.[48] The PTR/CARS data presented here show that $batho^{RT}$ has a completely different vibrational structure than that of Rh^{RT}. Of special note are the out-of-plane motions observed in the strong HOOP modes.

The high S/N found in the PTR/CARS results also ensures that a unique set of parameters characterizing bandwidth (Γ), band origin frequency (Ω), and amplitude (A) can be derived to represent the vibrational degrees of freedom assignable to both Rh^{RT} and $batho^{RT}$. These $\chi^{(3)}$ fitting parameters are presented in Tables 1 and 2.

1. Rise and Decay of $Batho^{RT}$. From transient absorption measurements on Rh^{RT},[49,50] the formation of $batho^{RT}$ has been shown to have a 3−7-ps rise time and is observed to decay with a 100-ns constant.[8] The time-dependent band intensity changes in these PTR/CARS data are consistent with the measured rise and decay times and provide the first opportunity to measure the vibrational structure of $batho^{RT}$ throughout its lifetime.

PTR/CARS spectra measured between 0 ps (8 ps CCT) and 104 ns demonstrate that the vibrational structure of $batho^{RT}$ remains unchanged between 10 ps and 104 ns. This structural stability is confirmed by data presented in Figures 5 and 6. PTR/CARS spectra, recorded at a 0 ps time delay, already contain pronounced HOOP bands that can be assigned to $batho^{RT}$ (Figure 5). These PTR/CARS spectra recorded at 0 ps, however, cannot be fit with the same set of $\chi^{(3)}$ parameters (including the electronic phase factor) derived only from the relative concentrations of Rh^{RT} and $batho^{RT}$ and their respective CARS spectra. This result indicates that another vibrationally distinct species (i.e., $photo^{RT}$) is present during the 8-ps CCT. The PTR/CARS data recorded between 10 ps and 104 ns, however, can be fit well with a $\chi^{(3)}$ function representing only Rh^{RT} and $batho^{RT}$ with fixed relative concentrations. PTR/CARS spectra taken at time delays longer than 104 ns (data not shown) cannot be fit with the unique set of $\chi^{(3)}$ parameters attributable only to Rh^{RT} and $batho^{RT}$. These last results indicate the presence of another Rh^{RT} intermediate (e.g., BSI).

From these data, it can also be inferred that no branching nor parallel processes producing structurally distinct intermediates are present during the early stages (10 ps−104 ns) of the Rh^{RT} photoreaction, i.e., prior to the decay of $batho^{RT}$.

2. Vibrational Spectra of Rh^{RT} and $Batho^{RT}$. It is noteworthy that, in general, the vibrational spectra from both Rh^{RT} and $batho^{RT}$ presented here are in excellent agreement with the corresponding RR spectra published previously. This is true for the frequencies of vibrational modes and for the overall pattern of vibrational features.

In detail, there are differences between the PTR/CARS results and a specific RR study. Specifically, in the fingerprint region of $batho^{RT}$ corresponds more closely with the results from one RR study[44] while the HOOP region agrees more closely with data from other RR studies (e.g., 850−cm^{-1}/858-cm^{-1} doublet).[28] Only low-intensity features in the region between the C═C stretching and the C═N stretching mode differ between the $batho^{RT}$ and the $batho^{LT}$ spectra. The significance of these different bands cannot be determined precisely since the PTR/CARS data in this region (near 1600 cm^{-1}) have a smaller S/N and a resultant error of >2 cm^{-1}.

In Rh^{RT}, the relative band amplitudes in PR/CARS, PTR/CARS, and RR data throughout the 700−1700-cm^{-1} region agree with each other. In PTR/CARS data from $batho^{RT}$, however, an approximately 1.5-fold increase in the amplitude of the C═C stretching band, relative to the intensities of the HOOP and fingerprint bands, is observed. This effect needs to be interpreted in terms of the respective relative intensities observed in RR spectra of $batho^{LT}$.

3. Rh^{RT} and $Batho^{RT}$ Vibrational Structure. Some understanding of the respective absolute vibrational structures of Rh^{RT} and $batho^{RT}$ can be derived from comparisons between the PR/CARS and PTR/CARS data and vibrational spectra obtained from the retinal chromophore in solutions. The vibrational spectra (700−1700 cm^{-1}) of *all-trans*- and 13-*cis*-retinal in solution have been analyzed extensively to determine characteristic vibrational patterns assignable to specific retinal structures isomers.[26,51] The corresponding RR spectra of the retinal chromophore in Rh, together with the analysis of isomeric retinal in solution, have established that the retinal configuration is 11-*cis*.

(48) Marcus, M. A.; Lewis, A. *Photochem. Photobiol.* **1979**, *29*,699−702.

(49) Popp, A.; Ujj, L.; Atkinson, G. H. *J. Phys. Chem.* **1995**, *99*, 10043−10045.

(50) Yan, M.; Manor, D.; Weng, G.; Chao, H.; Rothberg, L.; Jedju, T. M.; Alfano, R. R.; Callender, R. H. *Proc. Natl. Acad. Sci. U.S.A.* **1991**, *88*, 9809−9812.

(51) Curry, B.; Palings, I.; Broek, A.; Pardoen, J. A.; Mulder, P. P. J.; Lugtenburg, J.; Mathies, R. *J. Phys. Chem.* **1984**, *88*, 688−702.

The primary source of vibrational information pertaining to the isomeric structure of retinal is derived in RR spectra of the pigment from the fingerprint (C−C stretching) region. Specifically, the 1166-cm^{-1} batho^{LT}/batho^{RT} band, assigned to the $C_{10}-C_{11}$ stretching mode,[29] indicates that the *all-trans* geometry of the retinal is present in batho^{RT}. Five additional bands, at 1180, 1208, 1226, 1242, and 1276 cm^{-1}, are identified in the PTR/CARS batho^{RT} spectrum that are consistent with an *all-trans*-retinal. For comparison, the four C−C stretching bands characteristic of Rh^{RT} are at 1191, 1216, 1239, and 1268 cm^{-1} ($HC_{11}=C_{12}H$ in-plane rock).

CARS data recorded at RT demonstrate that the C=N stretching mode maintains a constant wavenumber position at 1654 cm^{-1} in both Rh^{RT} and batho^{RT}, while the C=C stretching mode shifts from 1545 to 1533 cm^{-1}. The validity of these observations has been discussed extensively,[44,52,53] but they now appear to be firmly established for both the Rh^{LT} and Rh^{RT} photoreactions. The constancy of the C=N stretching mode frequency indicates that batho formation does not significantly alter the Schiff-base modes. The 12-cm^{-1} shift of the C=C stretching mode in batho is consistent with the Rh^{RT} to batho^{RT} formation.

In the HOOP region of the batho^{RT} spectrum, four strong and five weak bands are observed, indicating a highly twisted (along the polyene chain) chromophore.[28] The dramatic increase in these HOOP modes upon batho^{RT} formation clearly demonstrates the largest structural difference between Rh^{RT} and batho^{RT}. Only one strong HOOP band at 972 cm^{-1} is found in Rh^{RT}. On the basis of the assignments of the 972-cm^{-1} band to the $HC_{11}-C_{12}H$ HOOP mode (*cis*),[27] it has been concluded that steric hindrance between the C_{13}-methyl group and $C_{10}-H$ exists in Rh^{RT}.

Seven Rh^{RT} and six batho^{RT} bands are identified in the CH_3 rock region between 1000 and 1100 cm^{-1} (Tables 1 and 2), of which five have analogous features (within 3 cm^{-1}) in both (Rh^{RT} and batho^{RT}) species (Figures 1−4). In Rh^{RT}, the 1000- and 1018-cm^{-1} bands can be assigned to the C_{13} and C_9 methyl groups, respectively.[26] The $\chi^{(3)}$ analysis of PR/CARS data reveals one more band for Rh^{RT} at 1010 cm^{-1}. The corresponding batho^{RT} bands are located at 1007 and 1018 cm^{-1}, respectively.

4. Energy Storage/Transduction Mechanism. (a) C=C Stretching Frequency versus Absorption Maxima. A schematic comparison of the positions of vibrational bands assigned to the C=C stretching modes in Rh and batho (at both RT and LT) with the respective absorption maxima at LT (77K) and RT are presented in Figure 7. The C=C stretching band in batho^{LT} appears 13 cm^{-1} shifted to lower energy relative to that of Rh^{LT}, while the formation of batho^{RT} from Rh^{RT} is accompanied by a 12-cm^{-1} shift to lower energy (PTR/CARS data, Figures 2 and 4). The results presented here correct earlier PTR/CARS data that showed the Rh^{RT} to batho^{RT} shift to be only 2−3 cm^{-1} [18] (*vide supra*).

These frequency shifts in vibrational features correlate well with changes in the visible absorption spectra maxima assigned to the Rh to batho transformation at RT (31 nm) and at LT (38 nm). These comparisons suggest that both measurements reflect similar molecular behavior, namely, the changes in the delocalization of the π-electronic energy within the polyene chain. These results support a proposed inverse relationship between the C=C stretching frequencies in retinal and absorption maxima in the retinal-containing protein.[16,54]

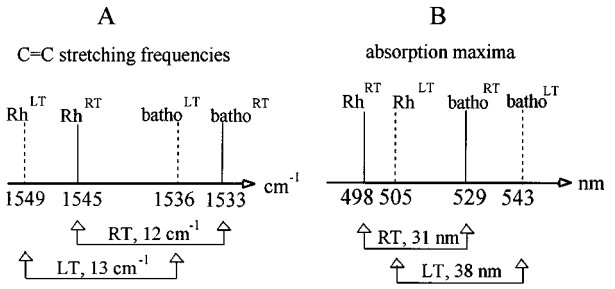

Figure 7. (A) Schematic comparison of the C=C stretching frequencies of Rh and batho at RT and LT. The value for Rh^{LT} are taken from Deng and Callender,[44] for Rh^{RT} from Mathies et al.[45] and Callender et al.,[46] and for batho^{LT} from Palings et al.[28,29] (B) Schematic comparison of the absorption maxima of Rh and batho at RT and LT. The values for Rh^{RT}, Rh^{LT}, and batho^{LT} are taken from Birge,[61] and the value for batho^{RT} is taken from Randall et al.[62]

(b) Schiff-Base Frequencies and Steric Constraints. The stretching frequency of the Schiff-base mode (C=N) remains unchanged when batho is formed from Rh under both RT and LT conditions. This constancy suggests that either (i) the counterion (e.g., Glu-113) is located at a significant distance from the positive charge on the Schiff-base proton ($N-H^+$) with which it interacts[52] or (ii) other dipoles within the protein maintain strong hydrogen bonding to the $N-H^+$ during batho formation (as evidenced by the large N-D^+ shifts).[55] The latter model is similar to that involving a salt bridge connecting the $N-H^+$ and the protein in Rh, which is replaced by hydrogen bonding to a neutral group when batho is formed.[44]

NMR data and semiempirical molecular orbital calculations place Glu-113 close to the C_{12} position (3 Å separation from C_{12} but not hydrogen-bonded to $N-H^+$) in Rh.[23] This location may provide a strong electrostatic interaction with the polyene chain of retinal and thereby may be associated with the unusually rapid isomerization rate.[12] By introducing $C_{11}-C_{12}$ isomerization and C−C single bond torsion along the polyene chain, the COO^- group of Glu-113 has been calculated to also lie near the retinal chromophore in batho.[23] This model places Glu-113 closer to an in-plane position with respect to the retinal while maintaining the 3 Å distance to C_{12}. One water molecule near the Schiff base also is predicted to be present and is possibly involved in hydrogen bonding to the Schiff base. The existence of such retinal/protein interaction, as well as its influence on the molecular mechanism, has been supported by studies of artificial Rh pigments. Studies on Rh^{RT} regenerated with structurally modified retinals that are selected to remove steric constraints produce different photoreactions and can diminish/abolish G-protein activation.[56] Other studies of Rh regenerated with structurally modified retinals have investigated reaction rates, quantum yields, the isomerization mechanism, and retinal/protein interactions.[31,57,58]

All of these data suggest that the retinal is located within a small, spatially constrained protein binding pocket. Upon the 11-*cis* to *all-trans* isomerization within retinal, new retinal−protein interactions lead to new spatial constraints and steric interactions between the retinal and the protein that must be

(52) Baasov, T.; Friedman, N.; Sheves, M. *Biochemistry* **1987**, *26*, 3210−3217.
(53) Livnah, N.; Sheves, M. *J. Am. Chem. Soc.* **1993**, *115*, 351−353.
(54) Doukas, A. G.; Callender, R. H.; Ebrey, T. G. *Biochemistry* **1978**, *17*, 2430−2435.
(55) Warshel, A.; Barboy, N. *J. Am. Chem. Soc.* **1982**, *104*, 1469−1476.
(56) Jäger, F.; Jäger, S.; Kräutle, O.; Friedman, N.; Sheves, M.; Hofmann, K. P.; Siebert, F. *Biochemistry* **1994**, *33*, 7389−7397.
(57) Nakanishi, K.; Crouch, R. K. *Isr. J. Chem.* **1995**, *35*, 253−272.
(58) Kochendoerfer, G. G.; Verdegem, P. J. E.; van der Hoef, I.; Lugtenburg, J.; Mathies, R. A. *Biochemistry* **1996**, *35*, 16230−16240.

associated with the 33 kcal/mol energy stored in batho.[5] The precise part(s) of the retinal (e.g., 9-methyl, 13-methyl, or β-ionone ring) contributing to these interactions remains to be determined.

Previously, the mechanisms proposed to describe energy storage in batho divided these contributions into charge separation and conformational distortions. For example, 20 kcal/mol has been attributed to conformational distortions and 12 kcal/mol to charge separation.[47] Alternatively, others have assigned only 3 kcal/mol to charge separation and 30 kcal/mol to conformational constraints.[59] The conformational constraints involved may arise from torsion along the polyene chain, displacement of the retinal backbone within the retinal plane (i.e., bending along the retinal axis),[59] or yet-unidentified retinal−protein interactions. The similarity of batho^{RT} and batho^{LT} vibrational structure suggest that all of these energy storage mechanisms should be considered applicable to the Rh^{RT} to batho^{RT} (*in vivo*) transformation.

(c) Temperature Dependence. Temperature-dependent effects are observable when the frequencies of the C═C stretching modes and the visible absorption maxima in Rh are considered (Figure 7). Based on an energy scale, temperature changes cause the vibrational frequencies in Rh (i.e., Rh^{RT} versus Rh^{LT}) and batho (i.e., batho^{RT} versus batho^{LT}) to move in the opposite direction to that observed in their respective absorption maxima (Figure 7). A shift to lower energy ("*red shift*") of 4 cm^{-1} in Rh and 3 cm^{-1} in batho is observed for the C═C stretching frequencies when the temperature increases from 77 K to RT. Correspondingly, a shift to higher energy ("*blue shift*") of 7 nm in Rh and 14 nm in batho of the visible absorption maxima is observed for a temperature increase. If the visible opsin shift is assumed to be caused mainly by changes in charge separation between N−H$^+$ and Glu-113, a decrease of the N−H$^+$/COO$^-$ distance in batho^{RT} relative to batho^{LT} would be anticipated. Since a *red shift* is observed in the C═C band position, however, another molecular change influencing the π-electron delocalization must occur. Such changes could include those that either alter the distance of the COO$^-$ group relative to the retinal (specifically, the C_{12} position) or alter the dipolar interactions of protein residues with the retinal. These PTR/CARS results, therefore, need to be included in any model describing the Rh → batho transformation, either at RT or at LT.

While maintaining similar molecular changes upon the formation of batho at RT and LT, the protein environment influencing retinal is different at RT versus LT. This is schematically illustrated in Figure 8, where shifts in absorption maxima and in the C═C stretching frequency are viewed in terms of the distances (Δ) between the Schiff base and the counterion Glu-113 [i.e., Δ(N−H$^+$/COO$^-$)] and between the retinal and counterion Glu-113 [Δ(C_{12}/COO$^-$)], respectively. In this model, only the C_{12} position of the retinal and the negative counterion Glu-113 are considered as probes for the retinal−protein interaction (a 15-*anti* configuration is assumed for both 11-*cis*- and *all-trans*-retinal). Decreasing Δ(N−H$^+$/COO$^-$) reduces π-electron delocalization, while decreasing Δ(C_{12}/COO$^-$) enhances π-electron delocalization.

To obtain an overview of how these molecular structure changes could influence vibrational and electronic data, the inverse relationship between the C═C stretching frequencies and the absorption maxima needs to be considered. The Δ(N−H$^+$/COO$^-$) and Δ(C_{12}/COO$^-$) values cannot decrease simultaneously if this inverse relationship is to remain valid. Since in this study the inverse relationship has been confirmed for Rh^{RT} and established for the first time for batho^{RT}, the Δ(N−H$^+$/COO$^-$) and Δ(C_{12}/COO$^-$) changes must be decoupled. Changes in Δ(N−H$^+$/COO$^-$) appear to determine the opsin shift, while changes in Δ(C_{12}/COO$^-$) influence π-electron delocalization.

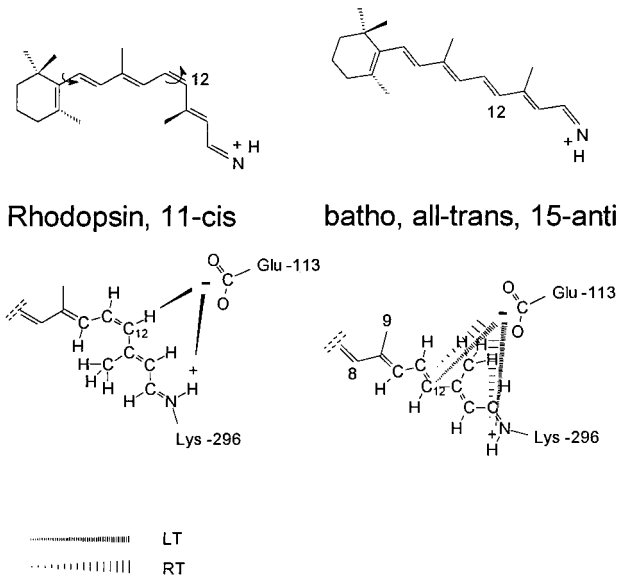

Figure 8. Schematic comparison of the retinal-protein interaction illustrated by the distance between C_{12} and Glu-113 (d(C_{12},COO$^-$)) and the distance between N−H$^+$ and Glu-113 (d(N−H$^+$/COO$^-$)). The solid arrows indicate that Glu-113 is located above the retinal plane, whereas the broken arrows indicate a position below the retinal plane. In batho^{RT}, (d(C_{12},COO$^-$)) and (d(N−H$^+$/COO$^-$)) are shorter as indicated by the changing width of the broken arrow.

In this context, it is also noteworthy that the more localized C═C stretching modes, appearing between 1580 and 1555 cm^{-1} (the C═N stretching mode), are observed at different wavenumber positions in RR and PTR/CARS spectra of batho, thereby indicating a different retinal environment along the conjugated chain. The S/N limitations ensure that only the 1561-cm^{-1} band can be considered to be significant; *vide supra*. No band near this position is observed in any batho^{LT} spectrum, thereby confirming that a different electrostatic environment exists for batho^{RT} versus batho^{LT}.

These PTR/CARS results make it evident that the retinal interaction between the retinal and the protein (e.g., Glu-113) in batho^{RT} is stronger than in batho^{LT}. If Glu-113 is involved, then electrostatic interactions are more prominent in the RT energy storage/transduction mechanism. Considering earlier results (especially from retinal-modified pigments), however, the major contribution to the energy storage/transduction mechanism (Rh to batho transition) still originates from steric interactions involving opsin and retinal (i.e., steric constraints). This appears to be correct even if the electrostatic interactions upon batho^{RT} formation are as much as twice those present upon batho^{LT} formation. Time-resolved infrared data may provide more insight into the role of specific retinal−protein interactions via measurements of individual protein vibrations (e.g., amide I and amide II bands). A protein backbone response of bacteriorhodopsin after laser excitation has been detected by picosecond IR transient absorption.[60]

Finally, it is interesting to note that different temperature effects are observed in the Rh^{RT} photoreaction and the BR^{RT}

(59) Smith, S. O.; Courtin, J. M.; Degroot, H. J. M.; Gebhard, R.; Lugtenburg, J. *Biochemistry* **1991**, *30*, 7409−7415.

(60) Diller, R.; Maiti, S.; Walker, G. C.; Cowen, B. R.; Pippenger, R.; Bogomolni, R. A.; Hochstrasser, R. M. *Chem. Phys. Lett.* **1995**, *241*, 109−115.

(61) Birge, R. R. *Biochim. Biophys. Acta.* **1990**, *1016*, 293−327.

photocycle. The formation of K-590 is accompanied by *blue shifts* in both the frequencies of the C═C stretching band and in the visible absorption maxima as the temperature increases from 77 K to RT.

Acknowledgment. This work was supported by an NIH research grant to G.H.A. F.J. is grateful to the Deutscher Akademischer Austausch Dienst for a DAAD/NATO postdoctoral fellowship. We thank Isaac Malagon, Anthony Mazza, Jr., and Hameed Shaukat for technical assistance and for the preparation of the rhodopsin samples.

JA9715298

(62) Randall, C. E.; Lewis, J. W.; Hug, S. J.; Björling, S. C.; Eisner-Shanas, I.; Friedman, N.; Ottolenghi, M.; Sheves, M.;Kliger, D. S. *J. Am. Chem. Soc.* **1991**, *113*, 3473−3485.